IRIS AperTO

UNIVERSITÀ DEGLI STUDI DI TORINO

AperTO - Archivio Istituzionale Open Access dell'Università di Torino

Crossing Electronic States in the Franck–Condon Zone of Carbon Dioxide: A Five-Fold Closed Seam of Conical and Glancing Intersections

This is the author's manuscript

Original Citation:

Availability:

This version is available http://hdl.handle.net/2318/137258 since 2016-10-06T14:08:49Z

Published version:

DOI:10.1021/jz301316y

Terms of use:

Open Access

Anyone can freely access the full text of works made available as "Open Access". Works made available under a Creative Commons license can be used according to the terms and conditions of said license. Use of all other works requires consent of the right holder (author or publisher) if not exempted from copyright protection by the applicable law.

(Article begins on next page)

12 October 2024

UNIVERSITÀ DEGLI STUDI DI TORINO

This is an author version of the contribution published on:

Sergy Grebenshchikov and Raffaele Borrelli. Crossing Electronic States in the Franck–Condon Zone of Carbon Dioxide: A Five–Fold Closed Seam of Conical and Glancing Intersections. *The Journal of Physical Chemistry Letters*, 3, 21, 2012, 10.1021/jz301316y.

The definitive version is available at:

http://pubs.acs.org/doi/abs/10.1021/jz301316y

Crossing electronic states in the Franck-Condon zone of carbon dioxide: A fivefold closed seam of conical and glancing intersections

Sergy Yu. Grebenshchikov[*,†] and Raffaele Borrelli[‡]

Department of Chemistry, Technical University of Munich, Lichtenbergstr. 4, 85747 Garching, Germany

E-mail: Sergy.Grebenshchikov@ch.tum.de

[*]To whom correspondence should be addressed

[†]Department of Chemistry, Technical University of Munich, Lichtenbergstr. 4, 85747 Garching, Germany

[‡]Permanent address: Dipartamento die Valorizzazione e Protezione delle Risorse Agroforestali, University of Torino, via Leonardo Da Vinci 44, Grugliasco (TO), Italy

Abstract

Intersections of electronic states are recognized as natural molecular hubs routing initial photoexcitation towards specific products. In this Letter, we investigate a five-fold intersection between the $2,3^1A'$ and $1,2,3^1A''$ electronic states of CO_2 responsible for the ultraviolet absorption of the molecule between 120 nm and 160 nm. It is demonstrated that the intersection is not an isolated point but a seam with the following properties: (1) The seam comprises both conical and glancing intersections; (2) The seam is a closed loop traced by the concerted displacements of two CO bonds; (3) The seam is constrained to linear geometries, and is purely planar; (4) The seam passes directly through the Franck-Condon zone. Topography and properties of the intersection seam are validated using assignment of the electronic wave functions and illustrated using circulation of the derivative couplings along closed contours. Possibility of observation of strongly curved seams is briefly discussed.

TOC Graphic

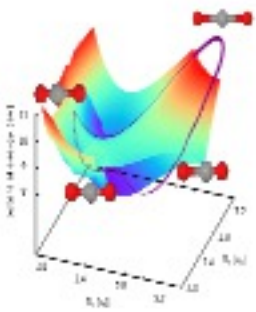

Keywords:

Conical intersections, Renner-Teller, intersection seam, non-adiabatic effects, carbon dioxde

Ultraviolet (UV) photodissociation of carbon dioxide[1] is of considerable importance for atmospheric, planetary, and interstellar chemistry and has received much attention of the experimentalists. Two diffuse bands, centered near 67 750 cm^{-1} (148 nm) and 75 000 cm^{-1} (133 nm), are particularly well studied, with the measurements covering the absorption profiles of irregular vibronic bands as well as the photofragment distributions in the singlet and triplet dissociation channels.[2–5] Theoretical studies[6–8] related the absorption maxima to the lowest excited valence states $1^1\Sigma_u^-$ and $1^1\Delta_u$ (the low energy band at 148 nm) and $1^1\Pi_g$ (the high energy 133 nm band).

Recently, the vibronic origin of the diffuse bands was established by solving the electron-nuclear Schrödinger equation for the first six interacting singlet electronic states, using full dimensional global potential energy surfaces (PESs) computed at a high level of ab initio theory.[9] The quality of ab initio PESs is manifested in the near spectroscopic accuracy of the calculated absorption spectra. The study demonstrated the significance of three strong non-adiabatic interactions in the Franck-Condon (FC) zone of the near-linear molecule: The rotoelectronic Renner-Teller (RT) effect in the orbitally doubly degenerate $^1\Delta_u$ and $^1\Pi_g$ states, the conical intersections (CIs) between $^1\Delta_u$ and $^1\Pi_g$, and the Herzberg-Teller effect in the transition dipole moments of $^1\Sigma_u^-$, $^1\Pi_g$, and $^1\Delta_u$ with $\tilde{X}\Sigma_g^+$. Carbon dioxide is photoexcited directly into the region of multiple degeneracies, with all excited states linked through a network of couplings created at RT intersections and CIs.

In this Letter, we investigate the topography of the intersecting states and demonstrate that all intersections are connected into a single seam which stretches over a substantial range of bond distances in the linear molecule. Recently, Levi et al. reported an extensive ab initio study of a seam of two-state CIs in methylamine.[10,11] The authors discovered a CI seam induced by a motion of a single proton in a well-specified molecular plane, conjectured that the seam should be closed, and gave heuristic arguments supporting this conjecture. Below we present direct numerical evidence of an intersection seam which comprises five optically active electronic states, is induced by atomic motion along one line, passes directly through the FC zone, and forms a closed loop.

Adiabatic energies of the first three $^1A'$ and the first three $^1A''$ electronic states, correlating at linearity with $\tilde{X}\,^1\Sigma_g^+$, $1^1\Pi_g$, $1^1\Sigma_u^-$, and $1^1\Delta_u$, are calculated on a dense three-dimensional grid

of CO bond distances $R_{1,2}$ and the bond angle α_{OCO}. Details of the calculations, carried out using MOLPRO package,[12] are available as Supporting Information. While PESs for the quantum dynamical calculations are constructed at the MRCI level of theory, the present work is mainly based on CASSCF calculations. The difference between two sets is quantitative but not qualitative: A closed intersection seam is found at both levels.

Analysis of crossings between calculated adiabatic states is indispensable in constructing an adequate quasi-diabatic representation for dynamics calculations. Two types of intersections with regard to their symmetry properties are identified in CO_2 [see Fig. 1(a,b)]:

Renner-Teller intersections[1] occur between one A' and one A'' state which become degenerate at linearity ($\alpha_{OCO} = 180°$). Among the six calculated states, two such pairs are present, corresponding to the orbitally degenerate $^1\Delta_u$ and $^1\Pi_g$ states [Fig. 1(a)]. The intersecting states remain degenerate as long as $\alpha_{OCO} = 180°$, and the 'degeneracy manifold' is the whole (R_1, R_2) plane.

Conical intersections occur inside A' or A'' symmetry blocks and stem from the $^1\Pi_g/^1\Delta_u$ crossing discovered by Knowles et al.[6,7] in linear CO_2 with bond distances $R_1^* = R_2^* \approx 2.2\,a_0$ [Fig. 1(b)]. At this geometry, the A' as well as A'' components of $^1\Pi_g$ and $^1\Delta_u$ intersect giving rise to two coinciding degeneracies in the (R_1, R_2) plane, one involving $2,3^1A'$ and the other involving $1,2^1A''$ or $2,3^1A''$ states. The intersections are conical because the degeneracies are lifted linearly along two orthogonal directions,[13] the bending angle α_{OCO} (symmetry breaking 'coupling mode'), and a combination of the two collinear stretches ('tuning mode') which for CO_2 is defined only locally.

The A' and A'' CIs occur not at one point (R_1^*, R_2^*), but along a line $F_{CI}(R_1^*, R_2^*) = 0$ in the (R_1, R_2) plane: The 'degeneracy manifold' is a one-dimensional seam,[13,14] CASSCF approximations to which are depicted in Fig. 2 for the states $2,3^1A'$ (red solid line) and $1,3^1A''$ (blue solid line). Results for both symmetries converge towards one single line of a fourfold crossing since the A' and A'' states are almost RT-degenerate. The residual discrepancy reflects the limited accuracy of CASSCF calculations. At the MRCI level, the A' and A'' seams are virtually in indistinguishable (green and black dash-dotted lines in Fig. 2)

A remarkable property of the calculated seam is that it traces out a closed isolated loop; this is

valid for both CASSCF and MRCI calculations. A CI seam can be viewed as a line of magnetic field flux whose vector potential $\mathbf{A}_n$ modifies the Hamiltonian for nuclear motion in the adiabatic electronic state $|n\rangle$ ('molecular Aharonov-Bohm' effect [15]). A closed loop in Fig. 2 is akin to the field of a toroidal magnet, with the equipotential lines of $\mathbf{A}_n$ encircling the seam in the bending plane perpendicular to the (R_1, R_2) plane. A closed strongly curved seam has several implications. 'Inconvenient' is that the tuning mode keeps changing its direction as the seam is traversed or that the popular local diabatization [16] has to give way to a global scheme. On the other hand, closed seams suggest that new interference phenomena should become observable (see below). Closed intersection seams were mentioned in several studies. For example, a triangular seam, formed by three crossing straight seams, has been reported for cyclic ozone. [17] A strongly curved intersection arch has been discovered in methylamine and assumed to be a part of a closed seam. [10,11] Our CO_2 study might be considered as a numerical demonstration of the validity of this assumption.

If the state $^1\Sigma_u^-$ (A'' symmetry block) is also considered, the Π_g/Δ_u seam in Fig. 2 has to be augmented with Π_g/Σ_u^- and Δ_u/Σ_u^- seams. The resulting picture is simplified by an accidental near-degeneracy between Δ_u and Σ_u^-: The Δ_u/Σ_u^- energy gap at linear geometries falls consistently below $300\,\mathrm{cm}^{-1}$ which is at the limit of the ab initio accuracy. Consequently, the Π_g/Σ_u^- seam (not shown in Fig. 2) is virtually indistinguishable from the Π_g/Δ_u seam. If the states Δ_u and Σ_u^- are assumed distinct, they cross along two straight lines cutting through the closed loop (blue solid lines parallel to R_1 and R_2 in Fig. 2). The intersection is glancing, since coupling via the bending mode is allowed only in the second order. [16,18] If the states Δ_u and Σ_u^- are assumed degenerate, the straight line seams dissolve into the (R_1, R_2) plane, while the Π_g/Σ_u^- and Π_g/Δ_u seams become identical. Counting two A' states, the seam in Fig. 2 represents therefore a fivefold degeneracy.

Topography of the fivefold seam implies the following diabatic Hamiltonian near linearity:[16,18]

$$\mathbf{H}^{(1,2)} = \mathbf{T}_{\mathrm{RT}} + \left(\begin{array}{cc|ccc} V_{\Pi'} & \alpha Q_u & & & \\ \alpha Q_u & V_{\Delta'} & & & \\ \hline & & V_{\Sigma\Delta''} & \beta Q_u & \gamma Q_u^2 \\ & & \beta Q_u & V_{\Pi''} & \beta Q_u \\ & & \gamma Q_u^2 & \beta Q_u & V_{\Sigma\Delta''} \end{array}\right) . \tag{1}$$

Here $\mathbf{T}_{\mathrm{RT}}$ is the 5×5 matrix of the rotoelectronic kinetic energy.[19] Diabatic states are labeled by the projection of the electronic orbital momentum L_z^2 on the molecular figure axis and by symmetry. Deviations from linearity are described using the coordinate $Q_u \sim \sin(\alpha_{\mathrm{OCO}})$ for which the lowest symmetry allowed order is kept. The potential matrix consists of a 2×2 block of A' and a 3×3 block of A'' states. The diabatic energies $V_{\Delta\Sigma''}$ of Δ_u and Σ_u^- are chosen degenerate; tiny adiabatic splitting can be recovered by adding off-diagonal second order terms $\sim R_1 R_2$. Due to orbital degeneracy, $V_{\Pi'} = V_{\Pi''}$ and $V_{\Delta'} = V_{\Sigma\Delta''}$, and the fivefold intersection seam is defined via

$$V_{\Pi'} = V_{\Delta'} = V_{\Sigma\Delta''} = V_{\Pi''} . \tag{2}$$

Diabatic potentials $V_{\Pi,\Delta}$ at linearity can be constructed by interpolation of the appropriately relabeled ab initio energies. The resulting smooth diabatic PESs are depicted in Fig. 1(c).

Up to now we deliberately avoided the discussion of how the closed isolated seam in Fig. 2 has been determined. Detection of degeneracies in the ab initio states can be far from straightforward.[17,20,21] Three different methods were used to validate our result, each giving a different perspective on the properties of the crossing states and the closed seam.

The basis of Fig. 2 forms the seam found from the numerical solution of Eq. (2) on a dense grid of CO bond distances and $\alpha_{\mathrm{OCO}} \approx 180^\circ$. Examples of adiabatic potentials $V_n(R_1)$ for three fixed R_2 values are shown in Fig. 3(a-c). The set of points at which the adiabatic potentials 'touched' [cf. Fig. 3(b,c)] was defined as an intersection seam. States are presumed to switch diabatic labels

upon passing the 'touching' point. Several approximations to the seam have been constructed in this way, all very much alike, for α_{OCO} ranging between 179° and 179.99°.

This approach, avoiding explicit diabatic assignments, becomes precarious for closed or strongly curved seams. Example is given in Fig. 3(a) and (b). In both frames the bond length $R_1 = 2.7\,a_0$ is perceived as an approximate intersection point, but only in (b) do the diabatic states actually cross. We re-examined the crossing seam and assigned each electronic state $|n\rangle$ with an expectation value $\langle L_z^2\rangle = \langle n|L_z^2|n\rangle$. Electronic assignments for states $2,3\,^1A'$ are summarized in Fig. 3(d-f) along the same cuts as in (a-c). Color coding is also taken from (a-c): Line of a particular color depicts evolution of the diabatic quantum number $\langle L_z^2\rangle$ for a particular adiabatic state. For example, the adiabatic states $2\,^1A'$ (blue line) and $3\,^1A'$ (red line) in Fig. 3(d) preserve their labels $\langle L_z^2\rangle = 1$ (Π_g state) and 4 (Δ_u state) along the cut in R_1. This cut, taken at $R_2 = 1.96\,a_0$, does not cross the seam but almost touches it at $2.70\,a_0$, and the observed avoided crossing is a mere curvature effect.[22] For $R_2 = 2.00\,a_0$, the cut passes twice through the seam, and the adiabatic states $2,3\,^1A'$ exchange their Π_g and Δ_u characters twice [Fig. 3(e)]. This means that the avoided crossing region in $V_n(R_1)$ hides two densely spaced intersection points. Further extension of R_2 drives the two intersections farther apart and makes them equally identifiable in $V_n(R_1)$ and $\langle L_z^2\rangle$ [Fig. 3(f)].

Crossings between A'' states [Fig. 3(g-i)] involve reorderings of three quantum numbers $\langle L_z^2\rangle =$ 0, 1, and 4, and the diabatic assignments are generally more difficult to follow. Along the 'tangent' cut in (g), the state $1\,^1A''$ (blue line) keeps its Π_g character without any crossings. The states $2\,^1A''$ (green line) and $3\,^1A''$ (red line) swap their labels $\langle L_z^2\rangle = 0$ and 4 at $R_1 = 2.71\,a_0$. This is an example of the glancing intersection between $^1\Sigma_u^-$ and $^1\Delta_u$. In the cuts (f,i), crossings are encountered between all three pairs Π_g/Δ_u, Π_g/Σ_u^-, Σ_u^-/Δ_u, and each integer $\langle L_z^2\rangle$ is passed over several states. However, since $^1\Sigma_u^-$ and $^1\Delta_u$ are degenerate, the sides $\langle L_z^2\rangle = 0$ and $\langle L_z^2\rangle = 4$ of the three-state diagrams can be glued together giving precisely the two-state diagrams of Fig. 3(d-f).

The seam of CIs can also be validated using 'topological' tests probing properties of electronic states transported along closed contours in the space of nuclear coordinates.[20,21,23] For real Hamiltonians one commonly seeks to detect the sign change in the adiabatic state, either directly (see

for example[13,15,17,24]) or — as in this work — using the circulation of interstate non-adiabatic coupling matrix elements, NACMEs $f_{nm}(Q) = \langle n|\frac{\partial}{\partial Q}|m\rangle$ (see for example[13,24–26]). To this end, a series of circular contours Γ_i in internal coordinates was constructed and parameterized using polar coordinates (ρ, φ). Examples in Fig. 2 include two contours normal to the seam plane (Γ_1 and Γ_2), and one lying in the seam plane (Γ_3). For each contour, angular NACMEs $f_{nm}(\varphi)$ and circulations

$$\Theta_{nm}(\Gamma) = \left| \int_0^{2\pi} \langle n|\frac{\partial}{\partial \varphi}|m\rangle d\varphi \right| \tag{3}$$

were evaluated using MOLPRO[12] for pairs of electronic states $|n\rangle$ and $|m\rangle$. Representative NACMEs for contours $\Gamma_{1,2,3}$ are shown in Fig. 4. Visualizing the intersection seam as a closed magnetic flux line with a vector potential $\mathbf{A}_n = \langle n|\frac{\partial}{\partial \varphi}|n\rangle$ helps to qualitatively understand the results. Indeed, the values of $\Theta_{nm}(\Gamma)$ are related to the geometric phases $\oint_\Gamma \mathbf{A} d\mathbf{l}$ acquired by the states along the contour Γ.[15,23] For two isolated states, zero geometric phase for either $|n\rangle$ or $|m\rangle$ implies zero $\Theta_{nm}(\Gamma)$; geometric phase of $\pm\pi$ for both states implies $\Theta_{nm}(\Gamma) = \pi$.[26] Since lines of the vector potential of a toroidal magnet are concentric circles centered on the flux line, any contour lying in the plane of the seam (like Γ_3) should give vanishing $\oint_\Gamma \mathbf{A}_n d\mathbf{l}$ and vanishing $\Theta_{nm}(\Gamma_3)$. Ab initio values along such contours are $\Theta_{23}(\Gamma_3) \approx 10^{-3}$ for states $2, 3A'$, and $\Theta_{nm}(\Gamma_3) \leq 10^{-1}$ for any pair of A'' states. On the other hand, if contours run along vector potential lines (like Γ_1 and Γ_2), $\oint_\Gamma \mathbf{A}_n d\mathbf{l}$ does not vanish. For $2, 3A'$, $\Theta_{23}(\Gamma_1) \approx 2.90$ and $\Theta_{23}(\Gamma_2) \approx 3.10$, i.e. reasonably close to π, and the calculated NACMEs are single-valued functions of φ [see Fig. 4(a)]. This demonstrates the local validity of the found seam for the two intersecting A' states. For A'' states, angular NACMEs and $\Theta_{nm}(\Gamma_{1,2})$ accurately predict three-state intersections. Indeed, NACME $f_{13}(\varphi)$ for the states $1^1A''$ and $3^1A''$ is a single-valued function of φ [see Fig. 4(a)] with $\Theta_{13}(\Gamma_1) \approx 3.10$. In contrast, NACMEs $f_{12}(\varphi)$ and $f_{23}(\varphi)$ in Fig. 4(b) are both double-valued with $f(\varphi + 2\pi) = -f(\varphi)$. This induced geometric phase effect of Han and Yarkony[26] is a manifestation of the Π_g/Σ_u^- and Σ_u^-/Δ_u intersections simultaneously enclosed by the contours $\Gamma_{1,2}$.[27]

While 'canonical' contours Γ_1 or Γ_2 provide excellent local tests, Baer and co-workers success-

fully used the zero circulation paths Γ_3 to locate the seam globally.[10,11] If such a contour crosses the flux line, NACMEs near crossings behave like delta functions;[11] positions of the delta peaks indicate points belonging to the seam [$f_{23}(\varphi)$ for the A'' states is shown in Fig. 4(a)]. Seam points located using Γ_3 contours with different centers and radii are shown in Fig. 2 with solid squares.

This work demonstrates, using symmetry arguments and direct ab initio computations, that the intersection seam of the first five excited singlet electronic states of CO_2 is constrained to linear geometries and forms a closed loop in the (R_1, R_2) plane. The seam passes through the FC zone (see Fig. 2) and is directly accessible via UV excitation. The Herzberg-Teller and Renner-Teller interactions, active in the FC zone, also perturb the vibronic bands, making a detailed analysis of non-adiabatic effects in the UV spectrum of CO_2 a challenging task.[9,28]

CIs are believed to provide a universal mechanism for ultrafast relaxation and possibilities of a direct optical detection of a CI are being actively explored (see e.g. Refs.[29–31]). What options are available for detecting a complete closed intersection seam? The ability to map out the coherent motion around the seam loop appears to be crucial but achievable for CO_2 only in the vacuum UV range since the potential difference along the calculated seam reaches 3.0 eV. At longer wavelengths, one might attempt to probe a curved seam 'locally'. CO_2 excited with UV light of wavelength $\lambda_{ph} \geq 120$ nm dissociates mainly into the spin-allowed channel $O(^1D) + CO(X^1\Sigma^+)$. Figures 1(b) and 2 demonstrate that as the CO bond elongates, the molecule passes through the curved seam twice and thus encounters two CIs separated by a distance R of the order of the seam curvature radius. At the first encounter, the initial excitation bifurcates into two components following the upper ($A_\uparrow$) and the lower ($A_\downarrow$) adiabats, with the lower subpacket further excited in the bending mode due to the geometric phase effect.[32] At the second encounter, the split components recombine into $\sim \left[A_\uparrow \exp(ik_\uparrow R) + A_\downarrow \exp(ik_\downarrow R)\right]$ and evolve towards the common product channel. Since bending vibration (the coupling mode) is active in transitions at both CIs, it is the oscillation patterns in rotational distributions of $CO(X^1\Sigma^+)$ which reveal the phase shifts $\exp(i\Delta kR)$ induced by the seam curvature R. There is growing evidence that a coherent passage through two CIs leads to measurable even-odd population oscillations in the fragment channels.[29,32] Detailed study of

such 'two double-slit' intramolecular interferometrs is an interesting subject for future research.

Acknowledgement

Financial support by the Deutsche Forschungsgemeinschaft is gratefully acknowledged. Authors would like to thank W. Domcke for useful discussions.

Supporting Information Available

Summary of the ab initio calculations. This material is available free of charge via Internet at http://pubs.acs.org.

References

(1) Herzberg, G. *Molecular Spectra and Molecular Structure III. Electronic Spectra and Electronic Structure of Polyatomic Molecules*; Van Nostrand: Princeton, 1967.

(2) Yoshino, K.; Esmond, J. R.; Sun, Y.; Parkinson, W. H.; Ito, K.; Matsui, T. *J. Quant. Spect. Radiat. Transf.* **1996**, *55*, 53.

(3) Zhu, Y.-F.; Gordon, R. J. *J. Chem. Phys.* **1990**, *92*, 2897.

(4) Chen, Z.; Lio, F.; Jiang, B.; Yang, X.; Parker, D. H. *J. Phys. Chem. Lett.* **2010**, *1*, 1861.

(5) Jackson, W. M. *private communication*.

(6) Knowles, P. J.; Rosmus, P.; Werner, H.-J. *Chem. Phys. Lett.* **1988**, *146*, 230.

(7) Spielfiedel, A.; Feautrier, N.; Cossart-Magos, C.; Chambaud, G.; Rosmus, P.; ans P. Botschwina, H. W. *J. Chem. Phys.* **1992**, *97*, 8382.

(8) Hwang, D.-Y.; Mebel, A. *Chem. Phys. Lett.* **2000**, *256*, 169.

(9) Grebenshchikov, S. Y. *J. Chem. Phys.* **2012**, *137*, 021101.

(10) Levi, C.; Halasz, G. J.; Vibok, A.; Bar, I.; Zeiri, Y.; Kosloff, R.; Baer, M. *J. Chem. Phys.* **2008**, *128*, 244302.

(11) Levi, C.; Halasz, G. J.; Vibok, A.; Bar, I.; Zeiri, Y.; Kosloff, R.; Baer, M. *Int. J. Quant. Chem.* **2009**, *109*, 2482.

(12) Werner, H.-J. et al. *MOLPRO, a package of ab initio programs*, 2003, see http://www.molpro.net.

(13) Yarkony, D. R. In *Conical Intersections*; Domcke, W.; Yarkony, D. R.; Köppel, H., Eds.; World Scientific: Singapore, 2004.

(14) Teller, E. *J. Phys. Chem.* **1937**, *41*, 109.

(15) Mead, C. A. *Rev. Mod. Phys.* **1992**, *64*, 51.

(16) Köppel, H.; Domcke, W.; Cederbaum, L. S. *Adv. Chem. Phys.* **1984**, *57*, 59.

(17) Atchity, G. J.; Ruedenberg, K.; Nanayakkara, A. *Theor. Chem. Acc.* **1997**, *96*, 195.

(18) Carter, S.; Mills, I. M.; Dixon, R. *J. Mol. Spec.* **1984**, *106*, 411.

(19) Petrongolo, C. *J. Chem. Phys.* **1988**, *89*, 1297.

(20) Longuet-Higgins, H. C. *Discuss. Faraday Soc.* **1975**, *35*, 77.

(21) Johansson, N.; Sjöqvist, E. *Phys. Rev. Lett.* **2004**, *92*, 060406.

(22) Paterson, M. J.; Bearpark, M. J.; Robb, M. A.; Blancafort, L. *J. Chem. Phys.* **2004**, *121*, 11562.

(23) Berry, M. V. *Proc. R. Soc. London, Ser. A* **1984**, *392*, 45.

(24) Baer, M. *Beyond Born Oppenheimer: Electronic Non-Adiabatic Coupling Terms and Conical Intersections*; Wiley: Hoboken, NJ, 2006.

(25) Mebel, A. M.; Baer, M.; Lin, S. H. *J. Chem. Phys.* **2000**, *112*, 10703.

(26) Han, S.; Yarkony, D. R. *J. Chem. Phys.* **2003**, *119*, 5058.

(27) Manolopoulos, D.; Child, M. S. *Phys. Rev. Lett.* **1999**, *82*, 2223.

(28) Grebenshchikov, S. Y. *unpublished* **2012**.

(29) Dixon, R. N.; Hwang, D. W.; Yang, X. F.; Harich, S.; Lin, J. J.; Yang, X. *Science* **1999**, *285*, 1249.

(30) Ashfold, M. N. R.; Cronin, B.; Devine, A. L.; Dixon, R. N.; Nix, M. G. D. *Science* **2006**, *312*, 1637.

(31) Lim, J. S.; Kim, S. K. *Nature Chemistry* **2010**, *2*, 627.

(32) Abe, M.; Ohtsuki, Y.; Fujimura, Y.; Lan, Z.; Domcke, W. *J. Chem. Phys.* **2006**, *124*, 224316.

Figure 1: Cuts through ab initio PESs along (a) OCO bond angle ($R_1 = R_2 = 2.2a_0$) and (b) one CO bond length ($R_2 = 2.2a_0$, $\alpha_{OCO} = 177^\circ$). In (c), CASSCF potentials for the diabatic $^1\Pi_g$ (blue) and $^1\Delta_u/^1\Sigma_u^-$ (red) states crossing along the closed seam are shown in the (R_1,R_2) plane ($\alpha_{OCO} = 179^\circ$). The lowest shown contour is 8.0 eV and the contour spacing is 0.25 eV.

Figure 2: The seam of conical and glancing intersections in the plane of the two CO bond distances R_1 and R_2 and $\alpha_{OCO} = 179.8^\circ$. CASSCF results are shown with red (A' symmetry) and blue (A'' symmetry) solid lines. MRCI results are shown with black (A') and green (A'') dash-dotted lines. Also shown are two branches of the glancing intersection between near degenerate $^1\Sigma_u^-$ and $^1\Delta_u$ states (straight solid blue lines). $\Gamma_{1,2,3}$ mark projections of the closed contours for angular NACMEs onto (R_1,R_2) plane. Contours $\Gamma_{1,2}$ are located in the plane of the bend and are normal to the (R_1,R_2) plane. Γ_1 is centered at $(R_1,R_2,\alpha_{OCO}) = (2.20a_0, 2.33\,a_0, 179.8^\circ)$; Γ_2 is centered at $(2.10a_0, 2.80a_0, 179,8^\circ)$; Γ_3 lies in the (R_1,R_2) plane and is centered at $(2.15\,a_0, 2.50a_0, 179,8^\circ)$. Solid squares indicate seam points obtained using NACMEs along the contours Γ_3. Grey blob indicates the FC point.

Figure 3: (a,b,c) CASSCF energies of the states $2^1A'$ and $1^1A''$ (blue), $2^1A''$ (green), $3^1A'$ and $3^1A''$ (red) versus CO bond distance. The second bond distance is fixed at $1.96\,a_0$ (a), $2.00\,a_0$ (b), and $2.40a_0$ (c). Bond angle is $\alpha_{OCO} = 179.8^\circ$. The state $2^1A''$ is artificially shifted by $400\,\mathrm{cm}^{-1}$ to lower energies in order to distinguish it from other states. Variation of the diabatic quantum numbers $\langle L_z^2 \rangle$ along the same cuts are shown in (d,e,f) for A' states and in (g,h,i) for A'' states (quantum number axis is placed on the right).

Figure 4: Ab initio angular NACMEs $f_{nm}(\varphi)$ along the closed contours versus polar angle φ. In (a), single-valued NACMEs are shown: $f_{13}(\varphi)$ (states $1^1A''$ and $3^1A''$, contour Γ_1, green line); $f_{23}(\varphi)$ (states $2^1A'$ and $3^1A'$, contour Γ_2, red line); $f_{23}(\varphi)$ (states $2^1A'$ and $3^1A'$, contour Γ_3, blue line). In (b), double-valued NACMEs are shown: $f_{12}(\varphi)$ (states $1^1A''$ and $2^1A''$, contour Γ_1, green line); $f_{12}(\varphi)$ (states $1^1A''$ and $2^1A''$, contour Γ_2, red line).

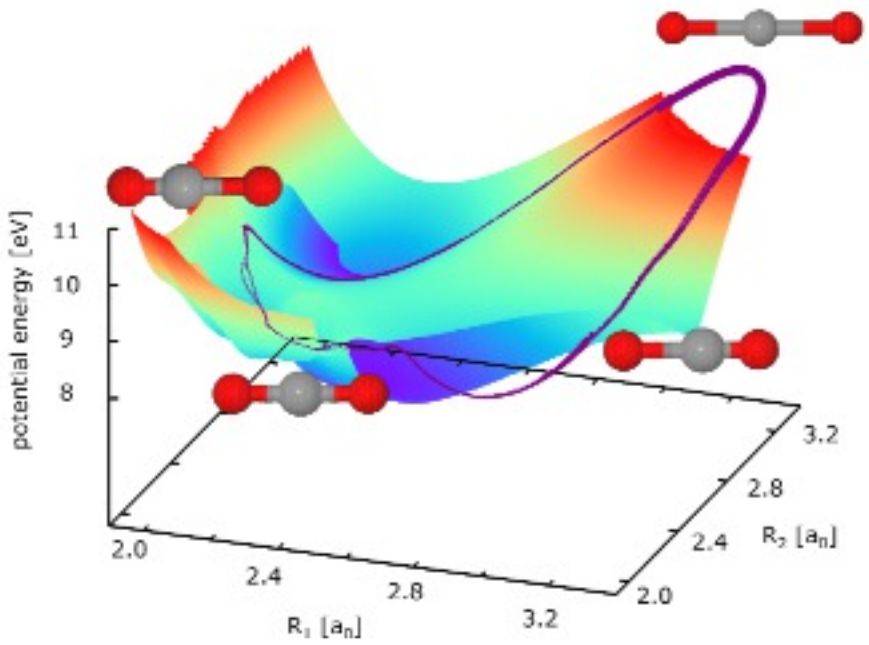

TOC Figure

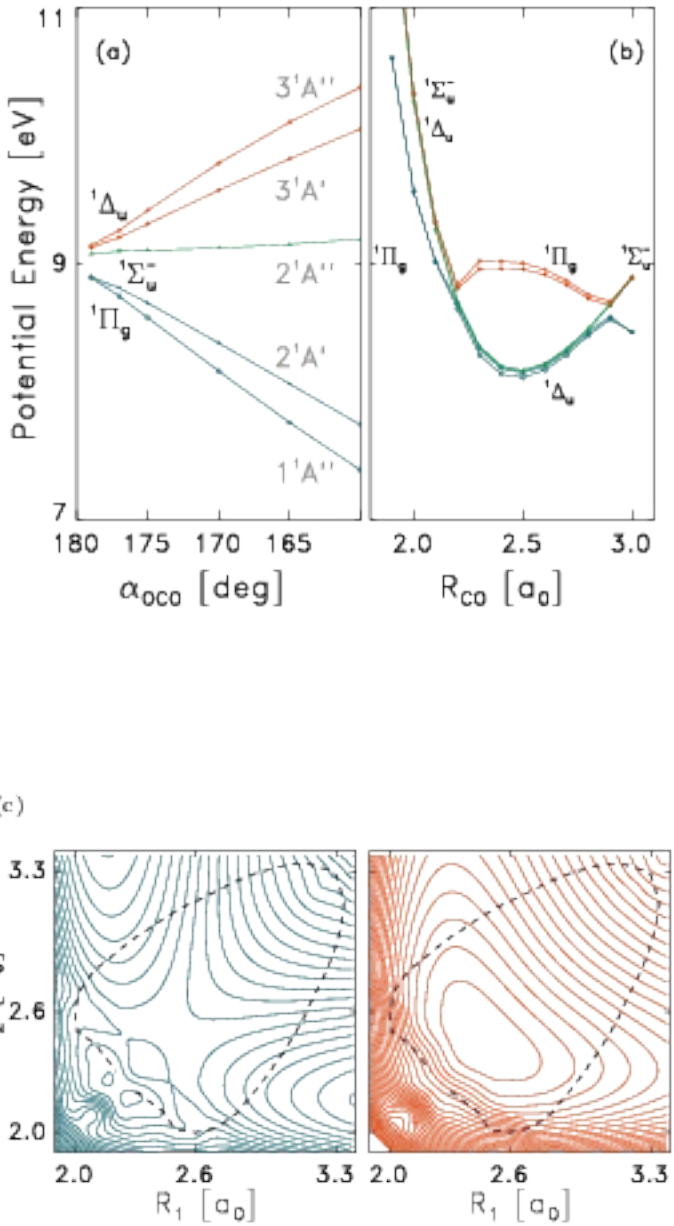
(a)
(b)
(c)
Potential Energy [eV]
11
9
7
180
175
170
165
α_{OCO} [deg]
2.0
2.5
3.0
R_{CO} [a_0]
3¹A''
3¹A'
2¹A''
2¹A'
1¹A''
¹Δu
¹Σu⁻
¹Πg
¹Σg⁻
3.3
2.6
2.0
R_2 [a_0]
R_1 [a_0]

Fig. 1

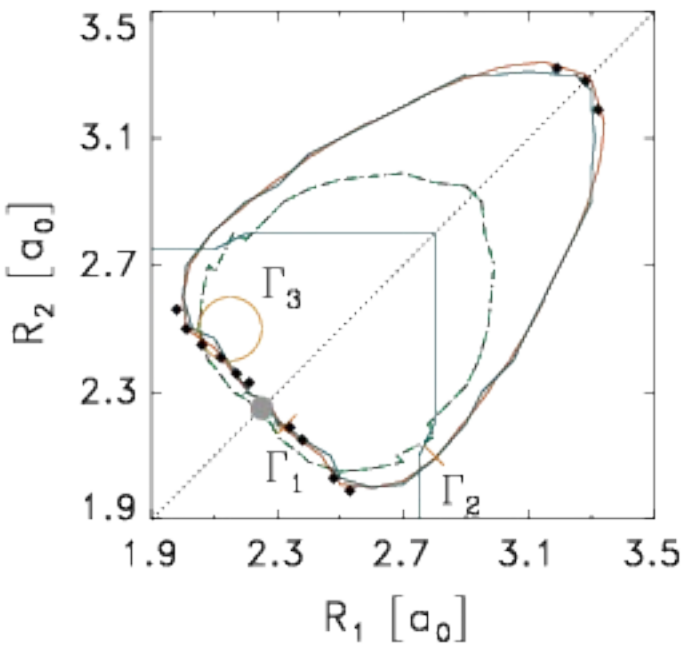

Fig. 2

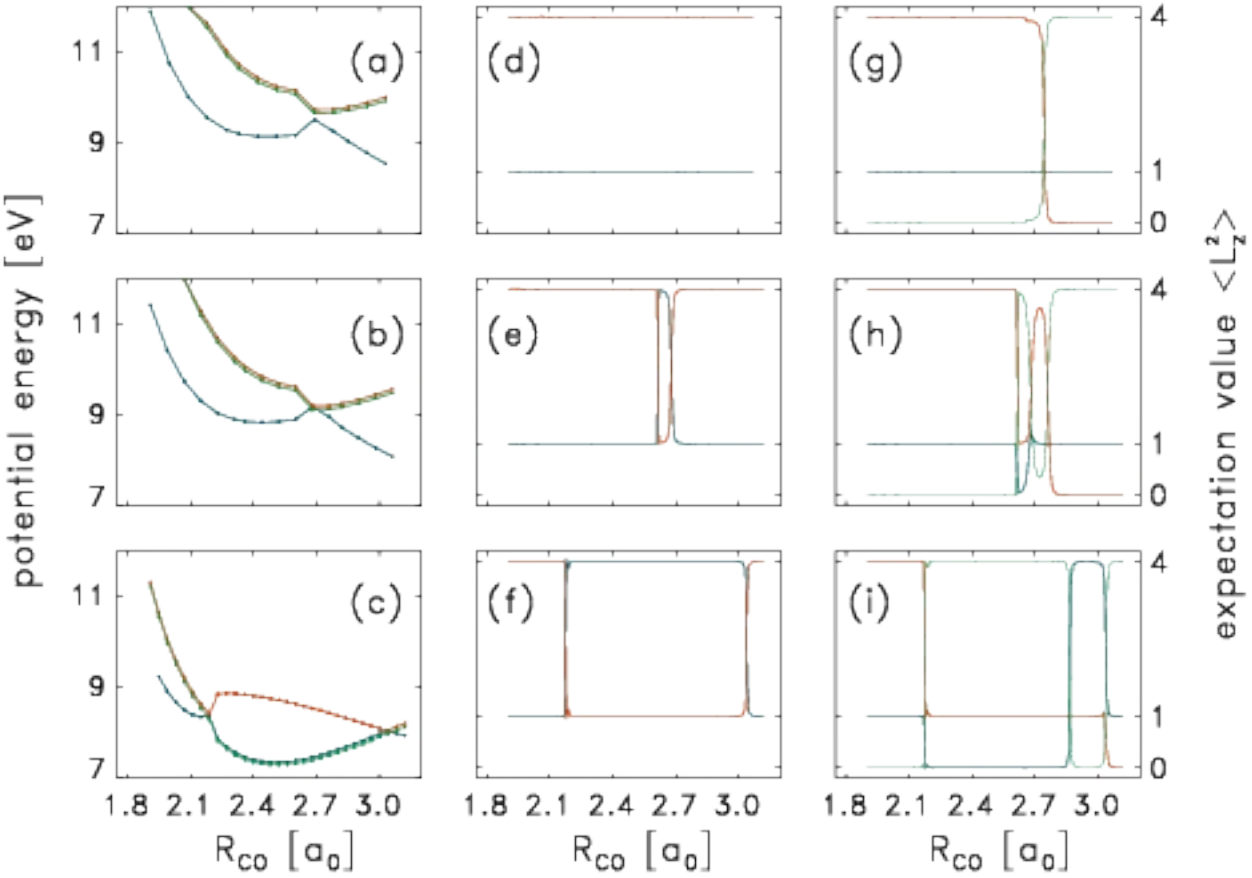
potential energy [eV]
expectation value <L_z^2>
(a)
(b)
(c)
(d)
(e)
(f)
(g)
(h)
(i)
11
9
7
4
1
0
1.8 2.1 2.4 2.7 3.0
R_CO [a_0]

Fig. 3

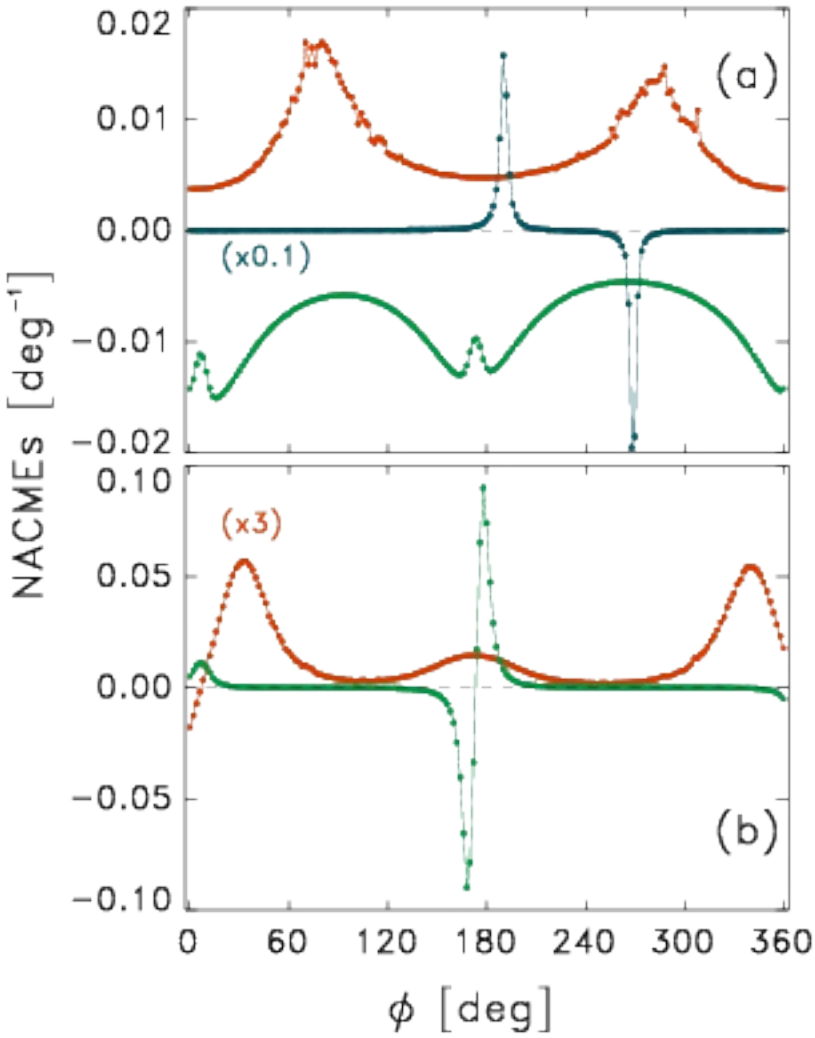

Fig. 4

This material is available free of charge via the Internet at `http://pubs.acs.org/`.